2021 43rd Annual International Conference of the
IEEE Engineering in Medicine & Biology Society (EMBC)
Oct 31 - Nov 4, 2021. Virtual Conference

Design of a Hyper-Spectral Imaging System for Gross Pathology of Pigmented Skin Lesions

Eleni Aloupogianni[1], Masahiro Ishikawa[2], Takaya Ichimura[3], Atsushi Sasaki[3], Naoki Kobayashi[2] and Takashi Obi[4]

***Abstract*— Pigmented skin lesions (PSL) are prevalent in Asian populations and their gross pathology remains a manual, tedious task. Hyper-spectral imaging (HSI) is a non-invasive non-ionizing acquisition technique, allowing malignant tissue to be identified by its spectral signature. We set up a hyper-spectral imaging (HSI) system targeting cancer margin detection of PSL. Because classification among PSL is achieved via comparison of spectral signatures, appropriate calibration is necessary to ensure sufficient data quality. We propose a strategy for system building, calibration and pre-processing, under the requirements of fast acquisition and wide field of view. Preliminary results show that the HSI-based system is able to effectively resolve reflectance signatures of ex-vivo tissue.**

***Clinical Relevance*—The imaging system proposed in this study can recover reflectance spectra from PSL during gross pathology, providing a wide imaging area.**

I. Introduction

Pathology laboratories endure heavy workloads and depend on personnel's expertise for effective diagnosis. As global population is adapting to remote work, digital pathology and telepathology is one of the fields that provide room for improvements. Specifically, for gross pathology, i.e. the intermediate stage of evaluating surgically extracted tissue prior to microscopical evaluation, the lack of automation is a significant bottleneck hindering the digital flow. A main hurdle in digitizing gross pathology is the inconsistency of image acquisition with a standard RGB camera, because color reproduction is affected by illumination conditions. This can be alleviated with the introduction of a Hyper-Spectral Imaging (HSI) system [1]. HSI is popular due to its non-invasive, non-ionizing properties and its ability to capture the spectral signature of particles comprising the tissue. Moreover, a detailed reflectance spectrum provides larger amount of information compared to the human eye, which integrates incident spectrum through the visual system's cone cells.

Skin cancer is the most common cancer in the United States and worldwide, representing the majority of skin cancer diagnoses in U.S., while it outnumbers other cancers combined [2]. More than 5,400 people worldwide die of non-melanoma skin cancer every month [3]. Regarding Asian populations, pigmented skin cancers at the appendages are the most commonly appearing skin cancers. Specifically, the most common ones in order of prevalence are Basal Cell Carcinoma at head and neck, Squamous Cell Carcinoma on the legs and Melanoma on covered surfaces (e.g. foot) [4]. Diagnosis of pigmented skin lesions (PSL) is a difficult task because malignancies at an early stage appear similar to benign morphologies.

Specifically for skin cancers, the main differentiating factor between malignant and benign skin lesions is peak height and shape of the measured spectrum [5]. Although HSI was developed originally for remote sensing applications, it has been employed in histological applications [6], as well as in dermatology, where systems targeting in-situ melanoma cancers exist both commercially [7] and experimentally [8], [9]. Nevertheless, dermoscopy remains the golden standard, because HSI-based systems suffer from false negatives and low specificity [10]. Furthermore, HSI-based systems for gross pathology are lagging behind, one of the obstacles being increased variability in colors, textures and shapes of the lesions among different pathologies. An effective HSI system targeting Asian populations should be able to handle multiple PSL types simultaneously, instead of only the melanoma-nevi dipole. HSI-systems at the grossing stage can facilitate tissue margin detection towards efficient histopathology [11] or telepathology [12]. Regardless, current HSI-based systems for gross pathology have low spatial resolution or limited field of view.

This study proposes a strategy for the setup and calibration of a 2D HSI system targeting gross tissue with PSL in Asian populations. The aim is to configure an acquisition system for margin detection during PSL diagnosis. In order to be incorporated in gross pathology practice, the system must meet requirements of large field of view and fast, noise-free acquisition. Additionally, the proposed system allows for higher spectral and spatial resolution than previous systems investigated for gross pathology of the skin. We present and evaluate the process towards system building, as well as normalization and pre-processing specifically for skin grossing. The proposed HSI system can assist diagnosis in detecting tumor margins through their spectral signatures.

II. Materials & Methods

A. Equipment

We investigated the setup of a HSI system targeting PSL of Japanese patients. The main component of the imaging system is a 2D spectroradiometer that can capture a 3D hyper-spectral image in the visible light range (Topcon SR-5000,

[1]Eleni Aloupogianni is with Department of Information & Communications Engineering, Tokyo Institute of Technology, Japan aloupogianni.e.aa@m.titech.ac.jp
[2] Faculty of Medical Care, Saitama Medical University, Japan
[3] Faculty of Medicine, Saitama Medical University, Japan
[4] Institute of Innovative Research, Tokyo Institute of Technology, Japan

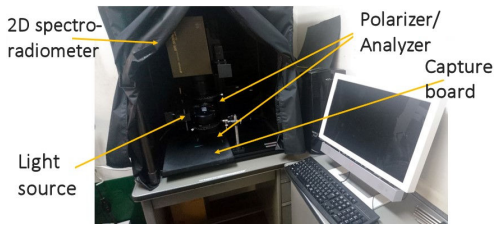

Fig. 1. The HSI acquisition system.

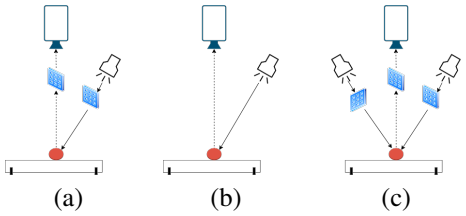

Fig. 2. Base configuration with (a) single light and polarizers, and experimental configurations (b) without polarizer pair and (c) with paired light source

1.4 mega pixel CCD image sensor, focal length: 32mm, spatial resolution: 1376x1024 pixel, range: 380-780nm, 32bit). The selected model is capable of high spectral resolution at 1nm. Regarding the light source, SOLAX-iO (SERIC LE-9ND55, LED, color temperature 5500K, $R_{15(skincolor)} = 99\%$) was selected, because it can render skin tones of Asian skin faithfully. We employed a Crossed Nicols configuration with paired polarizer and analyzer (TS High Contrast Plastic Polarizing Plate, Edmund Optics Japan, range: 400-700nm), in order to recover only transmittance modified by the intervening tissue sample. A white balance sheet (White Balance X-rite, July 2016 Edition) and a color chart target (Image Science Associates, ColorGauge Micro Target, Matte Version, 38mm x 45mm) were used as white reference and calibration target, respectively. Camera components were placed inside a black box that was tightly shut during capture. The complete HSI acquisition system is shown in Figure 1.

B. Strategy for System Building

At first, we focused on the components comprising the HSI capture system. The underlying assumption in system building is that the long-term goal is ability to handle not only gross tissue, but also in-situ tissue, thus requiring a large field of view. A base configuration with single light source and a pair of polarizers was compared to two experimental configurations as shown in Figure 2. Specifically, for the base configuration (Figure 2a), we set up a single illumination source, followed by a polarizing filter. The polarized rays are reflected on the target object, pass through the analyzing filter and reach the camera sensor. The spectroradiometer and the light source were positioned at 31.5m and 20cm from the capture board, respectively. The light source is tilted from the horizontal direction at 25°. In experiment 1, we evaluated the effect of Crossed Nicols configuration in pixel saturation and noise suppression. Base configuration was compared to an similar configuration without the polarizer/analyzer pair (Figure 2b). Imaging of fresh, moist tissue under direct light often results in highly-saturated patches on tissue surface. The goal is to investigate whether Crossed Nicols configuration succeeds in increasing the quality of the captured HSI by limiting incident light and consequently saturated pixels. In-situ moisturized hand tissue was used as capture target. In experiment 2, the use of single versus paired illumination source was evaluated in terms of imaging accuracy of the color chart tiles (1 pixel per tile). The base configuration is compared to a similar configuration with an additional light source and polarizing filter, symmetrical to the first light/filter pair (Figure 2c), in order to achieve uniform illumination of the capture board. The color chart was used as a capture target, and was imaged in a region of interest (ROI) of 266x320 pixels. After the main configuration is set, the angle of incidence rays arriving to the capture board is adjusted by tilting the light source. Use of the optimal angle for incident illumination reduces bias on spectrum peak height caused by the target‘s relative position on the capture board.

We investigated possible calibration settings assuming capture of ex-vivo fresh and damp tissue with maximum capture area 25x18cm. Acquisition time together with export time ranges from a few seconds to minutes, depending on the settings for capture ROI and imaging quality. Integration time is optimized according to target size and luminance, to provide accurate spectral measurements. Longer integration time means that light enters to the CCD sensor of the camera for longer time, increasing imaging duration. However, applications in gross pathology require fast imaging to avoid degradation of the fresh tissue due to prolonged exposure to the air. Therefore, after consultation with the pathologist, the compromise was managed by setting a 6-minute limit on total imaging time for tissue, including moving the specimen. The optimized settings during testing stage are used for subsequent imaging. The experiments in this study were approved by the Saitama Medical University Hospital Institutional Review Board (IRB) (17-128) and all participants gave informed consent for the scientific use of their data.

C. Data Acquisition

Since peak heights are a differentiating feature in skin malignancy classification, appropriate pre-processing is required. Although the spectroradiometer has a wider spectral range, limitations of other components prompt setting noise-free capture range to [420,730]nm with step 1nm. Depending on the Region of Interest (ROI) width and height, a measurement is a 3D matrix with size MxNx311. For each capture of tissue sample, I_T, we also capture the white reference, I_W, as well as a no-light reference, I_B. There are three available normalization options, with reference I_R calculated from I_W as: a) the spatial average spectrum over a region with high illumination intensity (Average), b) an artificial spectrum created from maximum measurements at each wavelength (Bandmax), c) the spectral measurement for respective (x,y) coordinates (Pixelwise). For the first two methods I_R is a

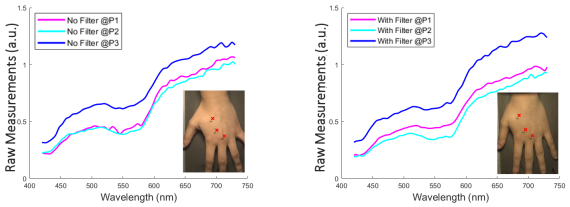

(a) (b)

Fig. 3. Normalized spectra (a) without polarizers, and (b) with polarizers.

vector, while for the latter it is a 3D array. Normalized measurements I are recovered with radiometric calibration

$$I_{(x,y)}(\lambda) = \frac{I_T(x,y,\lambda) - I_B(x,y,\lambda)}{I_R - I_B(x,y,\lambda)} \quad (1)$$

for pixel (x,y). In order to convert measurements to reflectance ratio in [0,1] value range, all spectra are multiplied with a constant coefficient. Given a finalized acquisition setup, the coefficient is calculated as follows. The color chart target is placed in the middle of the capture board and a normalized measurement for the white tile (Munsell W9.5) is recovered. The coefficient is calculated so that the normalized measurement converges at the same level as the standard measurement [13]. For display purposes, sRGB composites were created using raw measurements and the CIE color matching functions.

D. Evaluation

The HSI quality of our proposed configuration was evaluated in terms of measurement curve shape, as well as by comparison of the color chart measurements against 24 standard tile spectra [13]. Three pixel-wise metrics were used to quantify an equal number of criteria; Goodness-of-Fit Coefficient (GFC) for the curve shape, Normalized Mean Square Error (NMSE) for relative error, and Root Mean Square Error (RMSE) for absolute error, calculated as

$$GFC(obs,exp) = \frac{|r_{obs} \cdot r_{exp}|}{|r_{obs}|^2 |_{exp}|^2}, \quad (2)$$

$$NMSE(obs,exp) = \frac{\sum (r_{obs} - r_{exp})^2}{|r_{obs}|^2 |_{exp}|^2}, \quad (3)$$

$$RMSE(obs,exp) = \sqrt{\frac{1}{N} \sum (r_{obs} - r_{exp})^2}, \quad (4)$$

using normalized observed r_{obs} and expected r_{exp} measurements.

III. Results

During system building, the base configuration was evaluated against experimental configurations. For experiment 1, comparison between Pixelwise normalized skin spectra from in-situ imaging in Figure 3 showed that use of paired polarizers in Crossed Nicols setup led to smoother spectra and suppression of noise, especially in the green and red ranges. An sRGB reconstruction of the captured image shows that highly saturated pixels on the top left part of the hand,

TABLE I

Tile Spectra Comparison During System Building

Light Source	Normalization	GFC	NMSE	RMSE
single	Average	0.979	0.296	0.132
single	Bandmax	**0.983**	0.279	0.123
single	Pixelwise	0.981	**0.134**	**0.065**
double	Average	0.869	0.834	0.168
double	Bandmax	0.955	0.283	0.094
double	Pixelwise	0.872	2.385	0.176

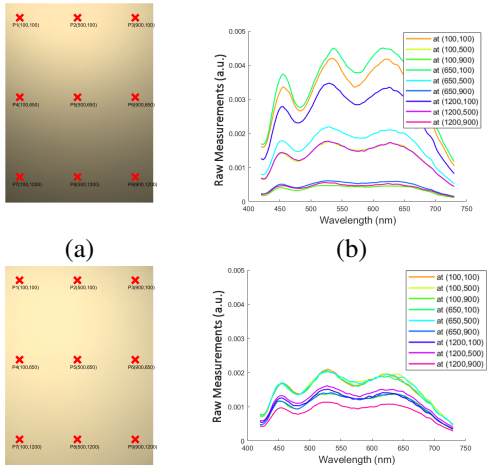

(a) (b) (c) (d)

Fig. 4. Selected pixels and raw spectral measurements for light angle and integration time set at (a),(b) 25°, 1360ms, and (c),(d) 40°, 618nm, respectively.

close to the light source, are suppressed to the level of the rest of the hand pixels. Regarding experiment 2, Table I shows average errors and GFC for 24 color chart tiles reflectance measurements against standard measurements. Base configuration with a single light achieves smaller error and higher GFC compared to paired-light sources. Additionally, Pixelwise normalization shows better agreement to the standard spectra.

From here onwards, base configuration is used. Sample stomach tissue was imaged ex-vivo to determine optimal integration time. Raw measured spectra for selected points on the white reference are shown in Figure 4. It is evident that the non-uniformity of incident illumination is affecting the height of measured spectral curves, despite the expectation that all points of the same material have the same absorbance. Optimal integration time is determined to be 1360ms, requiring in 5min to image a full 1376x1024 ROI. Adjustment of light angle to 40°alleviated the problem of illumination uniformity, reduced bias due to relative position of target and reduced optimal integration time to 618ms, effectively speeding up imaging to 3min. The color chart was imaged at the center and at the four corners of the capture board. Comparison of normalized tile spectra from the corners to measurements from the center is presented in Table II, described as mean ± standard deviation for the 24 tile measurements. Imaging with the light source tilted at

TABLE II

MEASUREMENT EVALUATION WITH RESPECT TO RELATIVE POSITION

Angle	Position	GFC	NMSE	RMSE
25°	BottomLeft	0.999±0.003	0.005±0.011	0.032±0.049
25°	TopLeft	0.999±0.001	0.004±0.006	0.025±0.008
25°	TopRight	0.999±0.001	0.005±0.009	0.031±0.012
25°	BottomRight	0.999±0.001	0.002±0.003	0.024±0.028
40°	BottomLeft	0.999±0.000	0.002±0.003	0.024±0.012
40°	TopLeft	0.999±0.001	0.007±0.020	0.028±0.014
40°	TopRight	0.999±0.001	0.009±0.023	0.029±0.017
40°	BottomRight	0.999±0.000	0.002±0.001	0.021±0.006

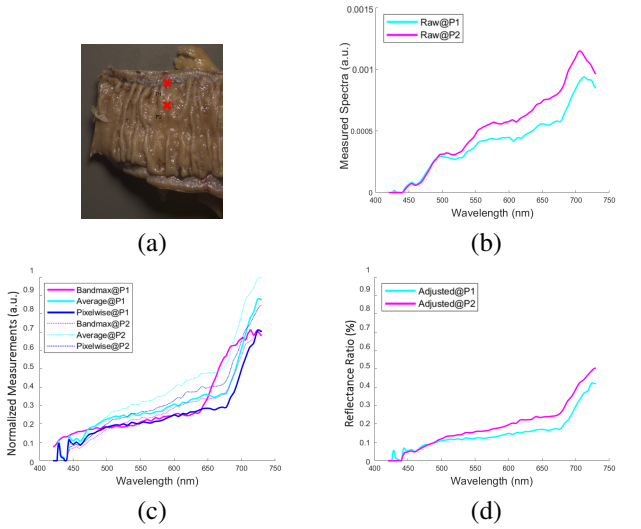

Fig. 5. For (a) two selected points on gross tissue, (b) raw, (c) normalized and (d) pre-processed spectra are shown.

40°results in improved values and smaller variance for GFC and RMSE for all relative positions of the target. Finally, raw measurements, normalized measurements and adjusted reflectances for two example pixels of ex-vivo stomach tissue are displayed in Figure 5. Bandmax normalization misrepresents the sudden slope hike of raw measurement at 700nm, while the other two normalization methods display it correctly. Regarding adjustment to reflectance ratio, the scaling constant was calculated at 0.595.

IV. DISCUSSION

In this study, a strategy for HSI system building and data extraction to assist gross pathology of PSL was presented. The two experiments during system building resulted in a configuration with single light source and polarizer pair being selected as optimal configuration. Measurements were normalized Pixelwise, because additionally to providing higher similarity to expected spectra, it is superior to the alternatives in terms of preserving the steep slope at 700nm in Figure 5c. Fast imaging at 618ms, well below the 6min cap, allows for additional recapturing in cases of a failure. Smaller ROI selection results in even smaller imaging duration. Shorter duration means that raw tissue properties are preserved, and that the influence of LED light flickering on noise is limited. It is shown that by tweaking the angle of the light source, average GFC and error values slightly improved, despite faster imaging duration, effectively suppressing bias from target position. The proposed HSI system faces limitations regarding minimum distance from the target, in order for sharp focus to be preserved.

The proposed HSI system will be used to create an original database of PSL, towards the development of a cancer margin detection system. Recovered reflectance spectra will be used together with learning algorithms for classification, in conjunction with Gaussian processes for fidelity estimation, to provide computer assisted diagnosis in skin gross pathology at first, and dermatology later.

ACKNOWLEDGMENT

We thank Hiroyuki Suzuki (Gunma University) for their valuable advice throughout this study.

REFERENCES

[1] M. Yamaguchi, H. Haneishi, and N. Ohyama, "Beyond Red–Green–Blue (RGB): Spectrum-Based Color Imaging Technology," *J. Imaging Sci. Technol.*, vol. 52, no. 1, p. 010201, 2008.

[2] "Cancer facts and figures 2021," American Cancer Society. [Online]. Available: https://www.cancer.org/content/dam/cancer-org/research/cancer-facts-and-statistics/annual-cancer-facts-and-figures/2021/cancer-facts-and-figures-2021.pdf

[3] C. Fitzmaurice, D. Abate, N. Abbasi, H. Abbastabar, F. Abd-Allah, *et al.*, "Global, Regional, and National Cancer Incidence, Mortality, Years of Life Lost, Years Lived With Disability, and Disability-Adjusted Life-Years for 29 Cancer Groups, 1990 to 2017," *JAMA Oncol.*, vol. 5, no. 12, p. 1749, dec 2019.

[4] H. M. Gloster and K. Neal, "Skin cancer in skin of color," *J. Am. Acad. Dermatol.*, vol. 55, no. 5, pp. 741–760, 2006.

[5] E. G. Borisova, T. I. Genova, P. P. Troyanova, E. P. Pavlova, I. Terziev, *et al.*, "Multispectral detection of cutaneous lesions using spectroscopy and microscopy approaches," in *Photonics Dermatology Plast. Surg. 2018*, B. Choi and H. Zeng, Eds., no. February. SPIE, feb 2018, p. 18.

[6] S. Ortega, M. Halicek, H. Fabelo, G. M. Callico, and B. Fei, "Hyperspectral and multispectral imaging in digital and computational pathology: a systematic review [Invited]," *Biomed. Opt. Express*, vol. 11, no. 6, p. 3195, jun 2020.

[7] G. Monheit, A. B. Cognetta, L. Ferris, H. Rabinovitz, K. Gross, *et al.*, "The performance of MelaFind: A prospective multicenter study," *Arch. Dermatol.*, vol. 147, no. 2, pp. 188–194, 2011.

[8] L. Rey-Barroso, F. J. Burgos-Fernández, M. Ares, S. Royo, X. Delpueyo, *et al.*, "Study of skin cancer lesions through multispectral and 3D techniques," *Opt. InfoBase Conf. Pap.*, vol. Part F142-, no. July 2019, pp. 8–13, jul 2019.

[9] R. Leon, B. Martinez-Vega, H. Fabelo, S. Ortega, V. Melian, *et al.*, "Non-Invasive Skin Cancer Diagnosis Using Hyperspectral Imaging for In-Situ Clinical Support," *J. Clin. Med.*, vol. 9, no. 6, p. 1662, jun 2020.

[10] L. Ferrante di Ruffano, Y. Takwoingi, J. Dinnes, N. Chuchu, S. E. Bayliss, *et al.*, "Computer-assisted diagnosis techniques (dermoscopy and spectroscopy-based) for diagnosing skin cancer in adults," *Cochrane Database Syst. Rev.*, vol. 53, no. 9, pp. 1689–1699, dec 2018.

[11] M. Halicek, J. D. Dormer, J. V. Little, A. Y. Chen, L. Myers, B. D. Sumer, and B. Fei, "Hyperspectral imaging of head and neck squamous cell carcinoma for cancer margin detection in surgical specimens from 102 patients using deep learning," *Cancers (Basel).*, vol. 11, no. 9, 2019.

[12] N. Kobayashi, H. Suzuki, M. Ishikawa, T. Obi, T. Ichimura, H. Yanagisawa, T. Tsuchida, and A. Sasaki, "Telepathology Support System with Gross Specimen Image Using High Resolution 4K Multispectral Camera," *Proc. Annu. Int. Conf. IEEE Eng. Med. Biol. Soc. EMBS*, vol. 2020-July, pp. 1388–1391, 2020.

[13] "Colorchecker rgb and spectra (april 2012)," Babel Color. [Online]. Available: https://www.babelcolor.com/colorchecker-2.htm